Lab on a Chip
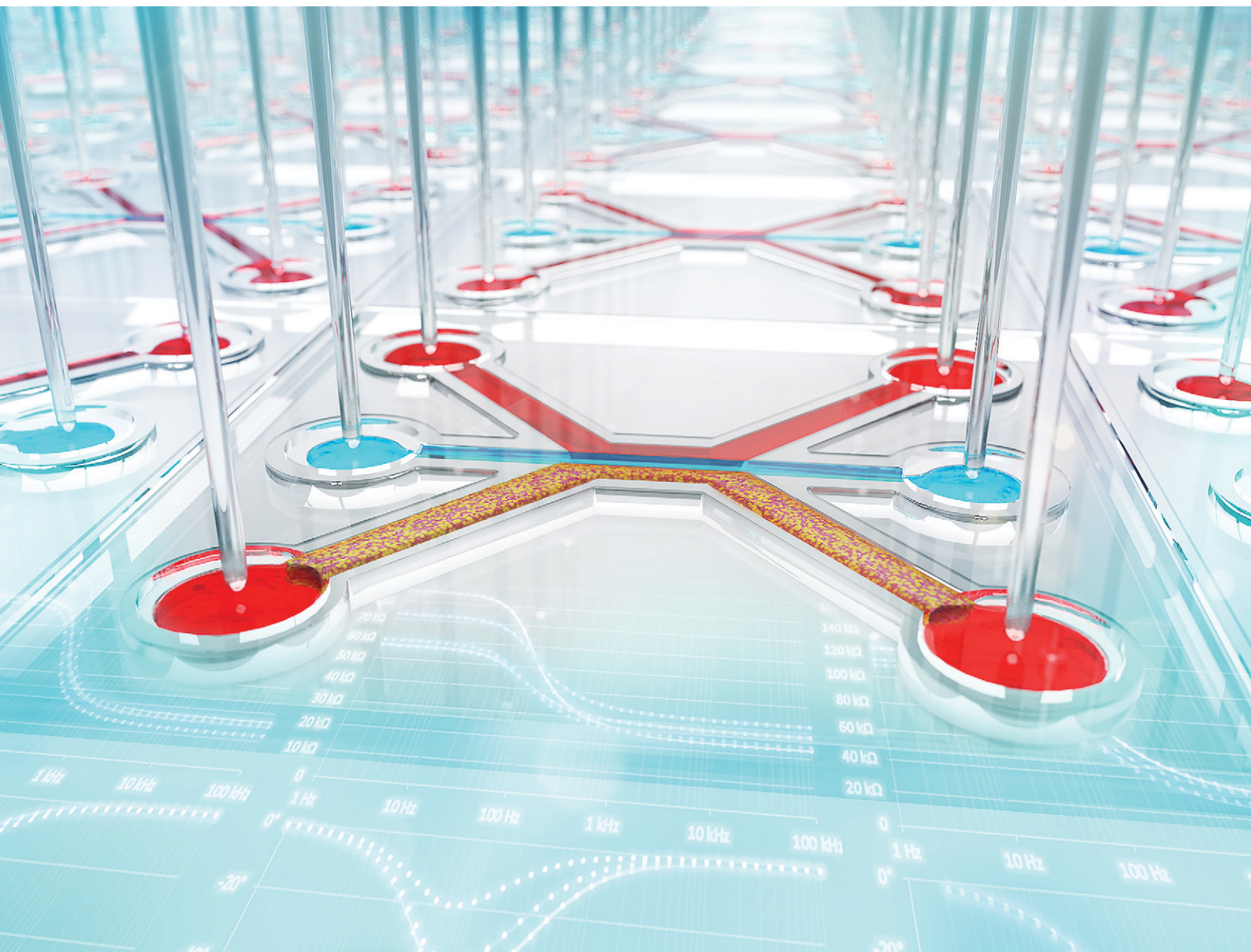
Devices and applications at the micro- and nanoscale

rsc.li/loc

ROYAL SOCIETY
OF CHEMISTRY

PAPER
Nicolas *et al.*
High throughput transepithelial electrical resistance (TEER)
measurements on perfused membrane-free epithelia

Lab on a Chip

PAPER

Check for updates

High throughput transepithelial electrical resistance (TEER) measurements on perfused membrane-free epithelia†

A. Nicolas, [iD] [ab] F. Schavemaker,[a] K. Kosim,[a] D. Kurek,[a] M. Haarmans,[a] M. Bulst,[c] K. Lee,[c] S. Wegner,[c] T. Hankemeier, [iD] [b] J. Joore,[a] K. Domansky,[a] H. L. Lanz,[a] P. Vulto[a] and S. J. Trietsch [iD] *[a]

Assessment of epithelial barrier function is critically important for studying healthy and diseased biological models. Here we introduce an instrument that measures transepithelial electrical resistance (TEER) of perfused epithelial tubes in the microfluidic OrganoPlate platform. The tubules are grown in microfluidic channels directly against an extracellular matrix, obviating the need for artificial filter membranes. We present TEER measurements on Caco-2 intestinal and renal proximal tubule epithelium. Forty tubules on one single plate were interrogated in less than a minute. We show that TEER measurement is significantly more sensitive than a fluorescent reporter leakage assay in response to staurosporine. We demonstrate a 40-channel time-lapse data acquisition over a 25 hour time period under flow conditions. We furthermore observed a 50% reduction in Caco-2 TEER values following exposure to a cocktail of inflammatory cytokines. To our best knowledge, this is the first instrument of its kind that allows routine TEER studies in perfused organ-on-a-chip systems without interference by artificial filter membranes. We believe the apparatus will contribute to accelerating routine adoption of perfused organ-on-a-chip systems in academic research and in industrial drug development.

Introduction

Barrier function of epithelia is crucial for maintaining homeostasis in the human body. Its disruption in organs such as the intestine, kidney, lung, skin, eye, or the blood–brain-barrier is a hallmark of numerous diseases and toxic effects.[1–3] Studying epithelial barrier function is essential for understanding disease processes, development of new therapeutic treatments, and investigation of compound safety. Permeability of epithelia grown *in vitro* is therefore routinely evaluated by fundamental and pharmaceutical researchers alike. In addition, proper barrier function is an important prerequisite when studying transport phenomena across epithelia *in vitro*.

Electrical measurement of the impedance is the gold standard for assessing the barrier function of epithelia *in vitro*. This so-called trans epithelial electrical resistance

(TEER) measurement correlates electrical properties of an epithelial layer with biological aspects such as cell layer confluency and thickness, tight junction formation, and morphology.[4]

Current systems for measuring TEER typically employ chopstick-like electrodes inserted into an electrolyte, usually a growth medium or a buffer solution, on both sides of a porous membrane insert.[4] An epithelial layer grown onto the porous insert is probed by an alternating current through the monolayer and measuring the associated electrical impedance. This impedance, once corrected for background offset and multiplied by the surface area of the insert, yields the TEER value of the tissue in $\Omega \text{ cm}^2$. Alternative methods include the use of surface-patterned electrodes on which an epithelial layer is grown.[5,6]

Over the last decade, the use of microfluidics-based cell culture systems, also called organ-on-a-chip systems, have rapidly gained popularity. These systems add physiologically relevant cues such as exposure to flow-induced shear stress, mechanical strain, and precise control of gradients. In addition, these platforms typically incorporate layered cell types of multiple lineages and include 3D extracellular matrix (ECM) components.[7]

TEER measurement capabilities have been implemented in a range of such microfluidic systems.[8] In 2017, Henry

[a] *Mimetas B. V., J.H. Oortweg 19, 2333CH, Leiden, The Netherlands.*
E-mail: s.trietsch@mimetas.com
[b] *Division of Analytical Biosciences, LACDR, Leiden University, Einsteinweg 55, 2333 CC Leiden, The Netherlands*
[c] *Scriospec GmbH, Leipziger Str. 43b, 04828 Bennewitz, Germany*
† Electronic supplementary information (ESI) available: Supplementary methodology and figures. See DOI: 10.1039/d0lc00770f

et al. reported a PDMS based microfluidic system with integrated planar electrodes designed for impedance spectroscopy.[9] Odijk *et al.* developed polydimethylsiloxane (PDMS) chips with embedded conductive biocompatible wires carrying the current close to the cell compartment.[10] TEER setups have been used to characterize models of tissues such as gut and blood–brain barrier.[11,12] Other reported solutions comprise either external porous inserts linked to perfused microfluidic channels[13,14] or artificial membranes directly built in the microfluidic devices.[15–17] The downside of these approaches lies in the limited scalability. Reported systems are typically based on single chips yielding single datapoints.[18–21] This makes it cumbersome to include dilution series, technical replicates, and controls.[22] Additionally, both on-chip and classical culture approaches make use of permeable membranes for culturing cells in barriers studies. While TEER values are usually area-corrected, complex current pathways are sources of non-biological variations, hampering interpretation. This makes the membrane a significant undesirable factor in the measurement process.[23–25]

Recently, we and others reported formation of perfused intestinal,[26–28] renal,[29–32] and vascular tubular barrier models.[33–37] In our studies, tubes were grown in a microfluidic titerplate called the OrganoPlate (Fig. 1a). Each chip comprises up to two tubules, grown directly against an
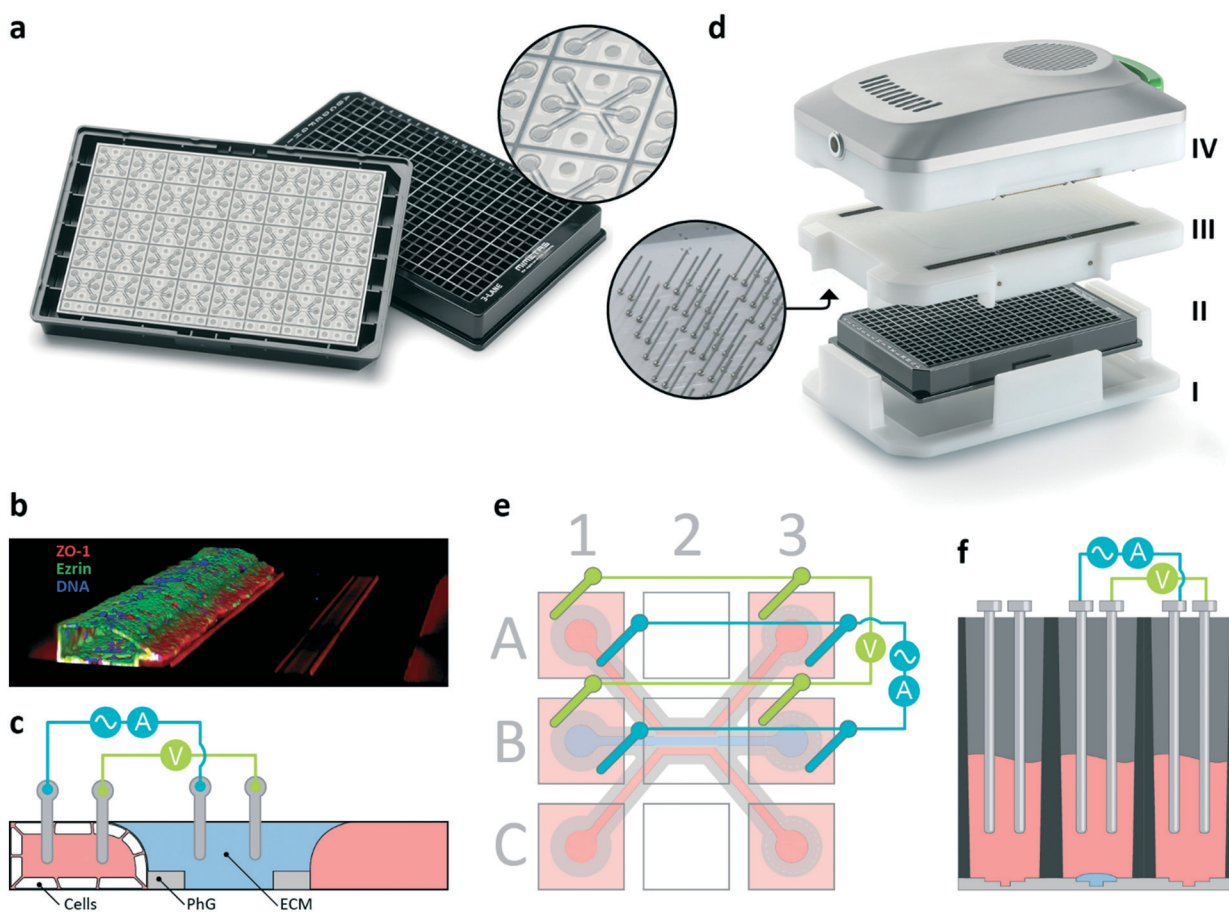

Fig. 1 OrganoPlate and OrganoTEER device design and measurement principle. (a) The OrganoPlate consists of a microtiter plate with 384 wells connecting to 40 microfluidic chips at the bottom of the plate. The inlay shows a single chip that comprises 3 channels that join in the centre of the chip. (b) A 3-dimensional reconstruction of a confocal image of a Caco-2 tubule cultured in the OrganoPlate. (c) Schematic cross-section of the centre of the chip, depicting the ECM gel, the phaseguides, the tube that is directly grown against the ECM gel, and a diagram of the electrical circuit formed from the apical to basal side of the tube. The two lanes adjacent to the ECM gel are perfused by passive levelling. (d) Exploded view of the OrganoTEER system including the plate holder (I), the OrganoPlate (II) in which the electrode board (III) is positioned and connected to the measurement module (IV). Further images shown in ESI† Fig. S2a–d. (e) Artist impression of electrode configuration addressing a single chip. Six squares represent access wells of the microtiter plate. To perform a four-point measurement in a single chip, eight electrodes are inserted in the four access wells. Electrodes on opposing ends of a lane are short circuited to form two electrode pairs: a current carrying pair (blue) and a voltage sensing pair (green). Short circuiting the electrode pairs results in lower resistance and more homogeneous current lines across the membrane. A controlled voltage source was connected between current carrying electrodes to impose a sinusoidal AC voltage of 100 mV amplitude across the microfluidic chip and the resulting current was measured. Voltage was measured between sensing electrodes to compensate for potential drop across the current carrying electrodes. Such four-point measurements are essential to remove low frequency effects due to electrical bilayers. Further electrical details and schematics are presented in ESI† Fig. S3a–c. (f) Schematic cross-section of three access wells with inserted electrodes. Electrodes dip in the medium, which acts as an electrolyte contacting the tube at either the luminal or basal side.

ECM, without the use of artificial membranes (Fig. 1b and c). Previously, we investigated barrier integrity by monitoring the leakage of a fluorescent reporter from the lumen of the tubule into the ECM. While this method is sensitive, scalable, and compatible with high content imaging platforms, it also requires several user interventions, including adding a fluorescent probe to the tubes in a timely manner. In addition, the assay is limited by the molecular size and weight of the fluorescent reporter and has limited compatibility with long-term time-lapse monitoring in general and under flow conditions in particular.[26]

Here, we report a methodology for measuring TEER of epithelial tubules in the OrganoPlate platform. The apparatus, called OrganoTEER, comprises 480 electrodes that dip into the wells of the microtiter plate, thereby contacting the cell culture medium that addresses either the luminal or basal side of the epithelium. We investigated TEER properties of the intestinal carcinoma cell line Caco-2 as well as the quasi-immortalized renal proximal tubule cell line RPTEC. Our measurements confirmed increasing TEER values with tubular growth over time and decreasing values in response to toxic compounds. We showed TEER to be more sensitive than a fluorescent reporter leakage assay and capable of time-lapse monitoring under flow conditions. Lastly, we demonstrated measurement of induced inflammation of Caco-2 tubules. The instrument is revolutionary in terms of its throughput, ease-of-use, and capability to interrogate epithelia under flow and without interference of porous membranes. We anticipate its routine use in both academic research and pharmaceutical development.

Materials & method

TEER device use and settings

The proposed TEER instrument consisted of four parts including a plate holder (i), electrode board (iii), measurement unit (iv) (Fig. 1d) and a laptop running drivers and analysis software (ESI† Fig. S1a and b). The electrode board, which was used to provide electrical connections to all chips in an OrganoPlate, featured 480 stainless steel electrodes integrated on a printed circuit board (see ESI† info S1.1). The stainless-steel electrodes were arranged in pairs to facilitate 4 terminal sensing. One electrode of each pair was current carrying while the other was voltage sensing. A controlled voltage source was connected between current carrying electrodes to impose a sinusoidal AC voltage of 100 mV amplitude across the investigated section of each microfluidic chip. Using the plate holder to ensure appropriate alignment, all electrode pairs were inserted directly into the inlet and outlet wells of the microfluidic channels of the OrganoPlate, forming individual electrically conductive paths across each chip through the respective ECM interfaces (Fig. 1c–f). The electrode board was connected to the measurement unit, which used a built-in impedance analyser capable of acquiring impedance spectra from 0.1 Hz to 1 MHz. A set of multiplexers was combined with a set of parallel, independently working, impedance analysers. This enables semi-parallel data acquisition, optimizing acquisition speed, and reducing heat generation. The assembly was connected to the laptop (i7 processor, 8 GB of RAM) via USB. Dedicated software controlled the measurement unit, recorded the data, and performed signal processing. The software allowed for optimization of the measurement parameters to the expected TEER values. The start and end frequencies could be chosen to match the system resistance and TEER. Lower starting frequency enabled measurement of higher TEER values at the cost of longer measurement times. Higher end frequencies, which are needed to measure lower TEER and the system resistance, had little impact on acquisition time. However, the useful range was limited by the parasitic capacitance. The precision setting of the internal analog-to-digital converter within the measurement module could be changed to adjust the integration time of points distributed across the frequency sweep. Higher values resulted in a higher signal-to-noise ratio (SNR) at the cost of slower acquisitions. Typical set values ranged between 0 and 1. The Averaging setting determined the number of sweeps across the spectrum. More sweeps could be averaged to increase the SNR at the cost of increased acquisition times. The most common setting was 1.

To accommodate long-term monitoring of TEER in an OrganoPlate, the OrganoTEER allowed for programming of time-lapse measurement series. Such series could include simple repeats, but also include more complex programs with the interval or frequency settings changing throughout the series. Carefully designed internal electronics with extremely low thermal output and component insulation enabled long-term use of the instrument inside a tissue culture incubator without negatively affecting the cells cultured in the plate or the functioning of the incubator. For single-point measurements outside an incubator, the OrganoPlate was taken out of the incubator, refreshed with 50 μL of cell culture medium and left to equilibrate at room temperature for 30 minutes prior to starting measurements. In contrast, all time-lapse TEER measurements were performed inside the incubator on a rocker.

Electrode board cleaning protocol

Before and after use, the electrodes were cleaned by spraying 70% ethanol onto the board using a spray bottle. The electrode board was left to dry for at least 30 minutes in a laminar flow cabinet. To minimize compound carryover following an exposure to a toxicant, we sequentially immersed the electrode board in 3 separate single well plates filled with Milli-Q water. After repeated use or long-term incubation with exposure of the electrodes to growth medium, fouling could be observed. To remove visible fouling of the electrodes, the electrode board was immersed in a single well plate filled with 50 mL of a 1:20 solution of RBS T342 (Chemical Products R. Borghgraef N.V, BE) in HBSS

(Sigma, DE, H6648). The electrode board was left in the solution for 15–20 minutes, after which the electrodes were rinsed with demi-water and left to dry ambiently.

Cell culture

Caco-2 cells (Sigma, DE, 86010202) were cultured in complete EMEM medium (ATCC, US, 30-2003) with 10% FBS (foetal bovine serum, ThermoFischer Scientific, US, 16140-071), 1% NEAA (non-essential amino acids, ThermoFischer Scientific, US, 11140050), and 1% penicillin (Sigma, DE, P4333), and harvested for experiments between passages 47 and 70. Renal proximal tubule epithelial cells (RPTEC, Kidney PTEC Control Cells, SA7K Clone, Sigma, DE, 44 MTOX1030) were cultured in MEME complete medium (Sigma, DE, M4526) with RPTEC complete supplement (Sigma, DE, MTOXRCSUP), L-glutamine at 1.87 mM (Sigma, DE, G7513), and amphotericin B at 14 ng ml^{-1} (Sigma, DE, A2942), and harvested for experiments at passage 3. All cells were cultured at 37 °C, 5% CO_2, 85% relative humidity (RH) while medium was refreshed every 2–3 days and cells were passaged or harvested at 80–90% confluency. Cells were resuspended at 10 000 cells per µL prior to seeding. 3-Lane 40 OrganoPlates (Mimetas, NL, 4003-400-B) were used to culture the organ-on-a-chip models presented in this work.

OrganoPlate 3-lane seeding

Tubules were cultured in a 3-lane OrganoPlate based on protocols previously described.[26] Briefly, ECM was prepared by mixing in 8:1:1 ratio collagen-I (5 mg mL^{-1}, AMSbio, GB, Cultrex 3D collagen I rat tail, #3447-020-01), HEPES (1M, ThermoFischer Scientific, US, 15630-122, pH 7.2–7.5) and $NaHCO_3$ (37 g L^{-1} Sigma, DE, H6648) on ice. The ECM mixture was kept on ice and used within 10 min. 3-Lane OrganoPlates were filled by dispensing 1.75 µL of the ECM gel into the gel inlet of each chip (Fig. 1e, well B1). The plates were incubated at 37 °C, 5% CO_2, and 85% RH for 15 minutes to let the ECM polymerize. After polymerization, 50 µL of HBSS (Sigma, DE, H6648) was pipetted in the gel inlet wells. The plates were placed in the incubator for further polymerization overnight. For tubule seeding, 2 µL of a cell suspension (10 000 cells per µL) was dispensed into the top perfusion inlet well (Fig. 1e, well A1), followed by 50 µL of medium. Tubes were seeded in 35 chips per plate, while cells were omitted in 5 control chips. The plates were incubated at a 75° angle to let the cells sediment against the ECM (see Fig. S4a and b†). After 2 hours, we verified that the cells were attached to the ECM by phase contrast microscopy and dispensed 50 µL of medium on the remaining perfusion inlets and outlets (Fig. 1e, well A3, C1 and C2). Perfusion was subsequently started by placing the plates on an interval rocker (OrganoFlow, Mimetas, NL) set at a 7° inclination and 8 minute interval inside an incubator. Medium was refreshed every 2–3 days.

Barrier integrity assay (BI assay) and apparent permeability (P_{app}) determination

Previously, we reported a method for assessing the barrier integrity of an OrganoPlate-grown tubule based on perfusing a tube with a fluorescent dye and observing its radial diffusion across the tubule into the ECM.[26] In short, complete cell medium was supplemented with 10 kDa FITC dextran (0.16 mg mL^{-1}, Sigma, DE, FD10S-100MG) and 155 kDa TRITC dextran (0.16 mg mL^{-1}, Sigma, DE, T1287-100MG) and added to the lumen of the Caco-2 tubules. The efflux of dextran into the adjacent ECM channel was monitored using a high content fluorescent microscope (ImageXpress XLS, Molecular Devices, US) in the FITC and TRITC channels using a 4× objective. The observation window with area of interest of each chip (Fig. 1e, well B2) was imaged every minute for 12 minutes. The images were processed by extracting the average fluorescence values of the top perfusion channel divided by the average fluorescence value of the gel channel for each chip and timepoint using the Fiji software.[38] This resulted in a curve of the normalized ratio of dextran in the gel channel over time (see ESI† Fig. S4c and d). We determined the apparent permeability (P_{app}) value using the following formula:

$$P_{app} = \frac{\Delta C_{receiver} \times V_{receiver}}{\Delta t \times A_{barrier} \times C_{donor}} \left(\frac{cm}{s}\right)$$

$\Delta C_{receiver}$ is the difference of the fluorescence intensity measured in the ECM channel between $t = 0$ and $t = 10$ minutes, $V_{receiver}$ is the volume of the measured region in the ECM channel ($h*w*l = 220$ µm × 2304 µm × 204 µm = 1.03 × 10^{-4} cm^3), Δt is the time between start and finish (10 minutes), $A_{barrier}$ (0.0057 cm^2) is the surface of the ECM interface with the medium channel, and C_{donor} is the fluorescence intensity measured in the top perfusion channel. This formula assumes linearity of the curve which is generally maintained when $C_{reciever}$ is below 10% of C_{donor}, as this means the concentration gradient and resulting flux is not significantly influenced by the increasing concentration in the receiver channel. The fluorescence intensity is assumed to be proportional to the concentration of the dextran dye, which is valid when the perfusion channel intensity does not oversaturate the image.

Toxicant exposure

For toxicant exposure experiments, Caco-2 tubules were seeded in a 3-lane OrganoPlate and grown to confluency over 4 days. Staurosporine (Sigma, DE, S440) was dissolved at decreasing concentrations (10 µM, 2.5 µM, 625 nM, 156 nM, 39 nM, 9.7 nM and 0 µM) in complete Caco-2 medium adjusted to 0.01% DMSO (Sigma, D8418-100ML). Prior to exposure, TEER measurements and a BI assay were performed on all chips. After the measurements, medium was substituted with medium containing the staurosporine concentration range, using 0.01% DMSO for control chips

without cells. Subsequently, the plate was placed in an OrganoTEER instrument, on an interval rocker, in an incubator (37 °C, 5% CO_2, 85% RH). A TEER time-lapse measurement was started immediately (t = 0) with measurements every 5 minutes for the first 40 minutes, and every 16 minutes afterwards until t = 155 min. A second BI assay was performed after 20 hours.

Inflammatory cytokine exposure

Caco-2 tubules were grown in an OrganoPlate as described above. On day 4 of culture in the OrganoPlate, cells were triggered for 72 h with medium containing TNFα (ImmunoTools, DE, cat. 11343015), INFγ (ImmunoTools, DE, cat. 11343536) and IL-1β (ImmunoTools, DE, cat. 11340013) at 100 ng ml^{-1} each for 72 h medium with compounds was added to all inlets and outlets.

Expression analysis

Total RNA of cytokine exposed Caco-2 tubules was extracted with the RNeasy Mini kit (Qiagen, DE, 74104) following the manufacturer's protocol, followed by reverse transcription using SuperScript™ IV First-Strand Synthesis System (Thermo Fisher, US, 18091050) or M-MLV reverse transcriptase (Thermo Fisher, US, 28025013) and random primers (Invitrogen, US, 48190011) according to manufacturer's protocols. Quantitative PCR was carried out on a Roche Lightcycler 96 using FastStart Essential DNA Green Master (Roche, CH, 06402712001). The following primers were used for amplification: IL-8 F: CAAGAG CCAGGAAGAAACCA, IL-8 R: ACTCCTTGGCAAAACTGCAC, ACTB F: CTCTTCCAGCCTTCCTTCCT, ACTB R: AGCACTGTGTT GGCGTACAG. Accompanying software (LightCycler® 96, Roche, CH) was used for the data analysis. Relative quantification was performed in all the analyses.

ELISA

After 72 hour inflammatory cytokine exposure, Caco-2 medium was collected and stored at −80 °C until the time of the assay. The concentration of IL-8 in the culture medium was measured using the Human IL-8/CXCL8 DuoSet (R&D Systems, US, DY208-05) according to the manufacturer's protocol.

Results

OrganoTEER setup

The OrganoTEER was designed to electrically interrogate cells cultured in the OrganoPlate. In this work, we report on measuring TEER in the OrganoPlate 3-lane. This OrganoPlate comprises 40 fluidically isolated and individually addressable chips integrated at the bottom of a 384 well plate (Fig. 1a). Each chip features three parallel lanes delineated by two phaseguides[39] on the bottom surface of the channel network (Fig. 1c, insert). The phaseguides constrain the ECM pre-cursor introduced into the chip to a defined lane by surface tension. Because the phaseguide-patterned ECM spans the entire conduit, it divides the conduit into three lanes: a central ECM lane and two flanking perfusion lanes. This patterning and subsequent gelation of the gel obviates the need for an artificial membrane barrier. Caco-2 cells seeded into one of the channels are let to form a tubule with a perfusable lumen (Fig. 1b). Gravity driven flow through the channels was achieved by placing the OrganoPlate on an interval rocker platform that tilted the plate at a given angle, which was reversed at determined intervals. The inlay in Fig. 1c shows an artist impression of a cross section depicting the phaseguides, the luminal side of the tube and the gel. A third lane was also perfused and provided fluid access to the basal side of the tube. Protocols for inducing Caco-2 cells to form tubular structures in the OrganoPlate 3-lane were reported by Trietsch et al.[26] and are summarized in Fig. S1a and b.†

Fig. 1d shows the OrganoTEER setup. The system consisted of four layers: a plate holder (i) to align the OrganoPlate (ii), an electrode board (iii) and a measurement unit comprising the electronics (vi). The electrode board comprised 480 electrodes dipping into 240 wells of the OrganoPlate (see Fig. 1c–f). Each electrode pair inserted into a single well comprises an actuation and a measurement electrode. The plate was placed in the plate holder and the electrode board was inserted on top with electrodes dipping into the medium in the wells of the OrganoPlate (see Fig. 1f). Subsequently, an electronic measurement module was attached to the electrode board through high density mezzanine connectors. The electronics comprise 12 independent impedance analysis units, connected to 80 tubes across 40 chips via a set of multiplexers, enabling rapid measurement of the impedance spectrum of all tubes on a plate.

Electrode pairs were inserted into the cell culture medium, which acted as an electrolyte addressing either the apical or the basal side of the tubules. Fig. 1c shows a cross section of the microfluidics well B2 with a conceptual drawing of how impedance was measured over the membrane. Fig. 1e shows a top view of electrodes addressing the luminal and the gel channel, respectively. Fig. 1f shows a cross-section of the entire plate along wells A1 B1 and C1 in. The electrodes inserted into the in- and outlets of the same tube were short circuited to leverage the symmetry of the setup, lowering the electrical resistance along the microfluidic channels. This increases the frequency range unaffected by parasitics. A video describing the setup and its handling is added as Video S1.†

The measurement unit was controlled via dedicated software as shown in ESI† Fig. S1a and b. The software allowed for simple selection of ranges of tubes or chips, as well as settings for time-lapse and measurement precision. The integrated impedance analyser was capable of measuring frequencies between 0.1 Hz and 1 MHz. The system, including software setup, could be assembled in less than a minute. Preconfigured protocols could probe 40 tubules, including data processing, in 45 seconds.

Depending on the required precision, parameters could be adjusted to balance speed and precision as required. The software allowed averaging of multiple datapoints as well as visualization of time-lapse measurement series.

To prevent undesirable heating of cultured cells, electronic components with minimal power consumption were selected and linked to an aluminium heatsink. To facilitate assembly of the OrganoPlate, the instrument features visual and physical guiding cues.

The OrganoTEER was designed to operate in the highly humidified environment of CO_2 incubators at 37 °C and minimally thermally load the incubator. For time-lapse measurements with cells under perfusion, the OrganoTEER could be secured on a tray of an OrganoFlow using an adapter.

Caco-2 and RPTEC TEER measurements

Impedance spectra of the gut Caco-2 and kidney RPTEC tubules were acquired at day 4 and 5 respectively after seeding (Fig. 2a and b). TEER values were determined by curve fitting through the measurement points in the 0.1 Hz to 1 MHz spectral range based on an equivalent circuit model described in Fig. S3b,† with the fitting methodology described in ESI† S1. TEER values were normalized to Ω cm^2 by multiplying the estimated resistance in Ω with the area of the ECM meniscus ($A_{barrier}$, 0.0057 cm^2). As depicted in Fig. 2c, Caco-2 tubules were found to have an average TEER value of 588 Ω cm^2, with a measured coefficient of variation (CV) of 1.36% (7.8 Ω cm^2). In contrast, the more permeable kidney proximal model RPTEC exhibited an average 6.4 ± 0.13 Ω cm^2 with a CV of 2.03% (0.13 Ω cm^2). These results show that the device can assess the integrity of tubules with a wide range of electrical properties. For both cell types, the coefficient of variation was quantified between 3 independent experiments, with a minimum of 10 technical replicates per cell type per experiment. The coefficient of variation for

technical repeats lies at 2% or lower depending on the absolute TEER value, showing robustness of both the biological model as well as the measurement system.

Real-time drug response testing

In a subsequent experiment, we assessed the barrier function of Caco-2 tubules in response to exposure to staurosporine. Staurosporine is a pan-kinase inhibitor known to disrupt the epithelial barrier. Previously, we reported increased leakage of a fluorescence marker upon exposure to staurosporine.[26] In this work, the fluorescent-based observations acquired after 24 h of exposure were compared with the TEER measurements (Fig. 3a) after 1, 6 and 24 hours of exposure, respectively. In addition, P_{app} values were calculated based on leakage of fluorescently labelled 10 kDa and 155 kDa dextran as illustrated in ESI† Fig. S4c and d. TEER values after 6 and 24 hours of exposure underwent a steep decline from 357 ± 21 Ω cm^2 at 0 mM and 6 hours to 0.1 ± 0.1 Ω cm^2 at 625 mM and 6 hours of staurosporine exposure. For 1 hour of exposure the decline in TEER was less pronounced, reaching a low plateau value of 52.6 ± 7.8 Ω cm^2 at 10 mM. In contrast, the P_{app} measurement following a 24 hour exposure showed measurable effects only for concentrations of 156 nM and above. Below this concentration, no significant difference in P_{app} was observed. This demonstrates that TEER is a significantly more sensitive measure of permeability modulation than assays based on fluorescent-reporters.

Next, we assessed real-time barrier disruption of tubules in a complete plate (35 tubules) over a period of 25 hours (Fig. 3b). Measurements were performed every 4 minutes for the first 45 minutes, followed by one measurement every 16 minutes for the subsequent 160 minutes and finally one measurement per 56 minutes until the end of the time-lapse. In the first 45 minutes, a steep decrease in TEER value for the three highest concentrations of staurosporine was observed, whereas the lower concentration remained stable, or even showed a small increase in TEER. For 1 to 3 hours a clear dose response could be observed, whereas for exposures longer than 5 hours all concentrations reached a plateau value. The time-lapse measurement showed a sawtooth pattern in high TEER values when the acquisition time is synchronized to the rocking motion of the plate (T = 0–0.75 and 2.7–24 h). It can be speculated the reversal of flow direction and peak of flow rate results in a short-term reduction of TEER, but non-biological effects such as changes in field line homogeneity due to changing liquid levels could also be a factor.

Measuring inflammation with TEER

To further evaluate the sensitivity of our TEER setup, Caco-2 tubules were exposed to a cocktail of pro-inflammatory cytokines. Increased permeability of the epithelial barrier and release of chemoattractant IL-8 from intestinal epithelium are common manifestations of inflammatory states found in disorders such as inflammatory bowel disease (IBD).[40–44] Here, a cocktail of cytokines comprising TNFα, IFN and IL-1β was used to induce inflammation. Upon 72 hour exposure,
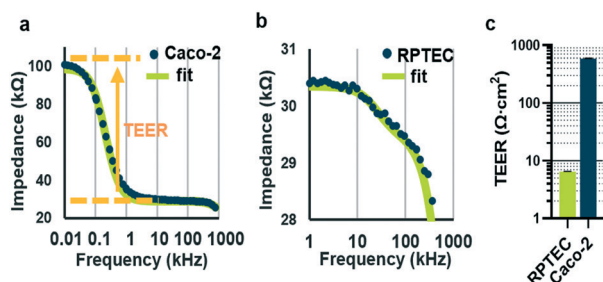

Fig. 2 TEER measured on Caco-2 and RPTEC (a) impedance spectrum of a Caco-2 tube on day 4. The orange arrow illustrates the contribution of the TEER to the spectrum. The fitted curve is based on an equivalent electrical model depicted as a simplified version in the ESI† S3b. The full methodology is presented in ESI† data S1.2 (b). Impedance spectrum and associated fitted curve of RPTEC tubule. (c) TEER values for Caco-2 and RPTEC tubes plotted with the coefficient of variation estimated across 3 independent plate measurements comprising at least 10 technical replicate each (N = 3, n > 10).
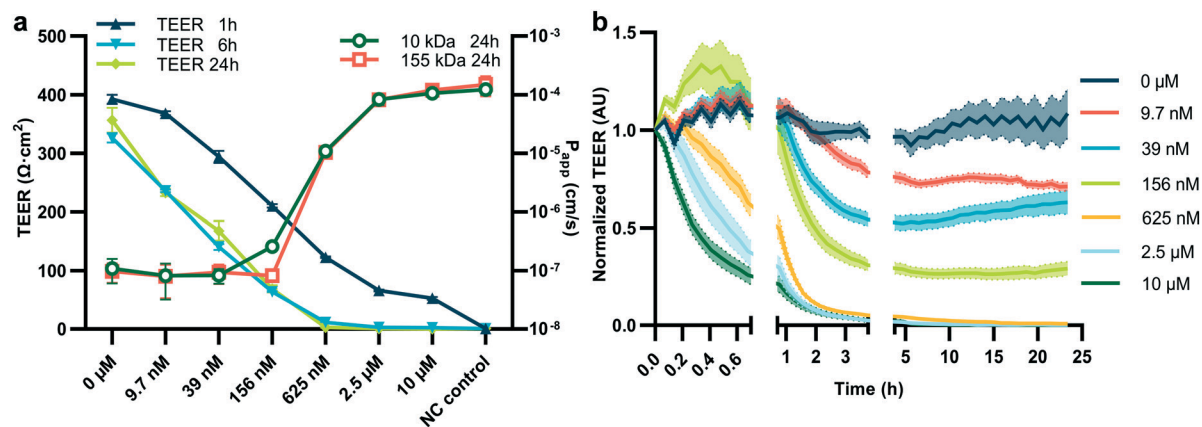
Fig. 3 TEER response to staurosporine. (a) TEER values at 1 h, 6 h and 24 h. For various doses of staurosporine, superimposed with bar graph of permeability to 155 kDa and 10 kDa dextran at 24 h. TEER data immediately pick up changes in permeability after lowest dose exposure of staurosporine, while fluorescent marker leakage picks up changes in permeability only for concentrations down to 156 nM. (b) Timelapse of TEER measurements on Caco-2 tubules upon staurosporine exposure. Measurements were taken in an incubator, while under rocker-based perfusion. Immediate response to high concentrations (625 nM, 2.5 µM and 10 µM) are visible within 40 minutes, whereas response to lower concentrations becomes visible upon 1–3 hours of exposure. Longer exposure results in plateau levels for all values. Curves are plotted with standard deviation of the mean as shaded area with the mean value as central line. Axis breaks indicate a change in sampling rate within the continuous acquisition. $N = 2$ and $n = 3–5$ for the TEER data as well as the P_{app} data.

TEER values of 4-day-old Caco-2 tubes were reduced by approximately 50% (Fig. 4a and b). Interestingly, in experiments reported previously, fluorescent reporter-based barrier integrity assays failed to pick up a reduction in barrier integrity in similar conditions.[45] To further investigate the inflammatory state of the epithelium, we assessed the release of IL-8 with ELISA and confirmed expression by qPCR (Fig. 4c and d). Both qPCR and ELISA showed a strongly increased production of IL-8 by the inflamed epithelial tubules that correlated with reduction in TEER values. The assays demonstrated high sensitivity and capacity of TEER for studying inflammation in the OrganoPlate.

Discussion and conclusion

We presented a technique for rapid TEER measurement of epithelial tubules in OrganoPlates using dip-in electrodes and impedance spectroscopy. The data acquisition parameters can be programmed to satisfy requirements of measurement speed and precision, as well as to accommodate long-term live cell monitoring in an incubator environment. Data acquisition and extraction was automated to increase consistency and throughput of measurements. We demonstrated the use of the device for assessing barrier function of Caco-2 and RPTEC tubes. We showed its
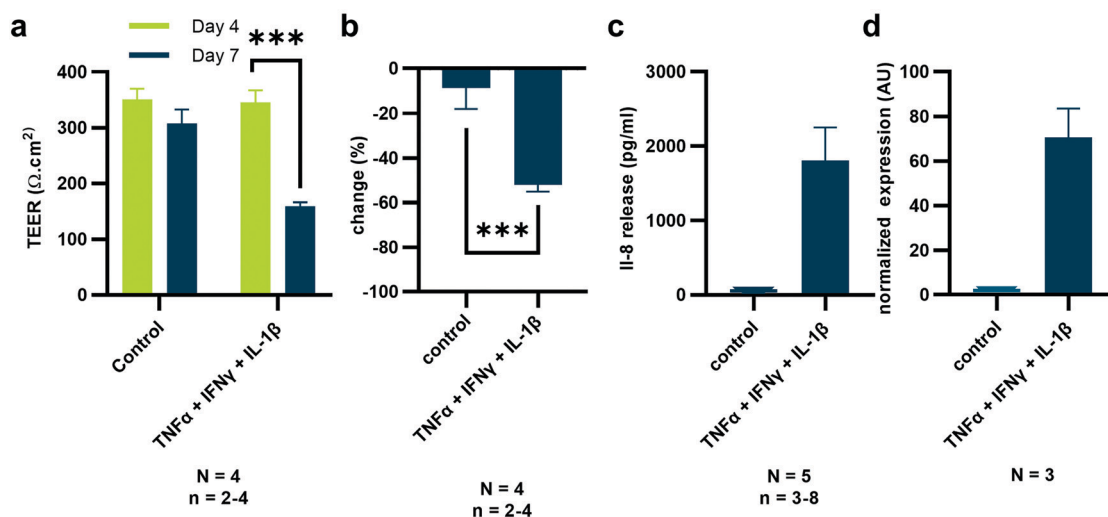

Fig. 4 Reduction of TEER values due to inflammation: TEER values of Caco-2 tubules before and after exposure to a cocktail of cytokines (TNFα, IFN and IL-1β) for 72 hours show significant reduction in TEER values both in absolute value (a) as well as percentage change (b). ELISA (c) and qPCR (d) analysis showed release and expression of IL-8 in response to cytokine treatment, confirming that tubes are in an inflamed state. All graphs are plotted using standard deviation of the mean. $N = 4$ and $n = 2–4$ for the TEER data, $N = 5$ and $n = 3–8$ for the ELISA. $N = 3$ for the qPCR data.

usefulness by presenting drug-induced time-lapse permeability measurements and demonstrated increased sensitivity in comparison to fluorescence-based leakage studies. Finally, we succeeded in electrically measuring induced inflammation effects in intestinal tubules.

The combination of 3D tube cultures without artificial membranes with TEER measurements, on 40 chips in parallel, is a unique feature of this platform. Using the OrganoPlate, cells are cultured directly against an ECM, which acts as an electrolyte. By not using a porous membrane, our setup allows to directly measure the TEER of the cell layer only, avoiding skewing the results by membrane characteristics such as pore size and density, as well as compensation for ECM coating and/or deposition. By removing the need to account for pore size in relation to cellular dimensions and ECM properties, we reduce the bias due to current line distribution in and around the cells, as well as potential bias induced by different methods for area correction of porous membranes.

The most common method for reporting TEER values is to generate area-corrected values in Ω cm^2 (as typically done for TEER measurements on membrane inserts). Here, we reported both area-corrected values as well as relative changes in TEER. The advantage of area-corrected values is that it allows for comparing values between different platforms. However, care should still be taken when interpreting these values as current density gradients could affect the measured values. As reported by Yeste, especially low TEER values could be overestimated, when the geometrical correction is not corrected for current density gradients.[46]

We observed much higher TEER values in the Caco-2 gut model than in the renal proximal tubules, a difference which is reflected in the physiological function of these organs. Kidney proximal tubules have TEER values ranging from 6 to 10 Ω cm^2 *in vivo*,[47] while TEER values of Caco-2 monolayers are typically around 400 Ω cm^2.[4] These known cell models serve as a good reference for our system's dynamic range and precision. The theoretical limit of detection of the OrganoTEER can be approximated based on the characteristic frequency f_c of a cell barrier. With an estimated parasitic cut-off frequency f_P of 100 kHz and cell capacitance estimated above 1 μF cm^{-2}, the theoretical limit of detection of our method would be approximately 1.6 Ω cm^2.

In this paper we have shown that the machine can measure 40 tubules in parallel. However, the apparatus is equipped to measure many more datapoints. For instance, the setup could measure two tubules per chip, measuring up to 80 tubules in parallel. Changing of the electrode board and OrganoPlate layout would even enable measurement of up to 128 tubules. These high numbers of tubules measured in parallel are important not only for industrial scale studies, but also for academic research. Availability of adequate number of datapoints to acquire proper controls and relevant numbers of technical replicates allows for performing TEER-based experimental studies with sufficient statistical power. As a result, a single experiment can yield significant results,

while reducing variation commonly introduced through multiplication of reagent preparation, handling, cell source and passaging.

Here we performed measurements on a single tubule per chip. However, we envision more complex models going forward. For instance, an endothelial and an epithelial barrier could be modelled and interrogated in a single chip. In such a setup, the first perfusion channel would comprise an epithelial tubule, whereas the second perfusion channel comprises a blood vessel. Such a setup allows to interrogate the two barriers separately, while still permitting cross talk between the tissues. We also anticipate the use of the measurement setup to assess slight variations in culture conditions induced by proliferation of cells as well as (*trans*) migration of cells over epithelial or endothelial membranes.

Live monitoring of cellular barriers is valuable in quality control of growing healthy tubules, as well as in investigation of toxicological, inflammatory, and pathological processes. The ability to monitor dozens of tissues in parallel, combined with the small footprint of the device makes it ideal as a primary readout in compound dilution series and large drug screens. We also envision future development including an automated setup, with either the OrganoPlate or the TEER device robotically manipulated to allow repeated measurements of multiple OrganoPlates. The measurement speed from a couple of seconds down to less than 0.1 second for a single chip offers unique ways of measuring fast kinetic effects. Potentially, resistance and capacitive measurements could open the door for active ion flow measurements.

In summary, we have developed a fast, easy to use tool for parallel TEER measurements in perfused epithelial tubules that are devoid of artificial membranes. The machine adds a tool to the organ-on-a-chip toolbox, allowing for routine adoption of the technology by any end-user in both academic as well as industrial settings. TEER measurements can be combined with other commonly used assays to complement physiologically relevant organ chip models with quantitative analysis for the development of better drugs and therapies.

Author contributions

A. N., P. V., and S. T. invented the OrganoTEER concept. A. N., F. S., P. V., M. B., K. L., S. W., K. D., and S. T. contributed to the design and engineering of the instrument and software. A. N., F. S., K. K., D. K., and M. H. planned, performed, and analysed experiments. K. D., T. H., H. L., J. J., P. V., and S. T. supervised the work and edited the manuscript.

Conflicts of interest

Acknowledgements

References

1 R. Cecchelli, V. Berezowski, S. Lundquist, M. Culot, M. Renftel, M. Dehouck and L. Fenart, *Nat. Rev. Drug Discovery*, 2007, **6**, 650–661.

2 M. Odenwald and J. Turner, *Nat. Rev. Gastroenterol. Hepatol.*, 2016, **14**, 9–21.

3 M. Wilmer, C. Ng, H. Lanz, P. Vulto, L. Suter-Dick and R. Masereeuw, *Trends Biotechnol.*, 2016, **34**, 156–170.

4 B. Srinivasan, A. Kolli, M. Esch, H. Abaci, M. Shuler and J. Hickman, *J. Lab. Autom.*, 2015, **20**, 107–126.

5 F. Asphahani and M. Zhang, *Analyst*, 2007, **132**, 835.

6 P. Secker, N. Schlichenmaier, M. Beilmann, U. Deschl and D. Dietrich, *Arch. Toxicol.*, 2019, **93**, 1965–1978.

7 V. van Duinen, S. Trietsch, J. Joore, P. Vulto and T. Hankemeier, *Curr. Opin. Biotechnol.*, 2015, **35**, 118–126.

8 B. Srinivasan, A. Kolli, M. Esch, H. Abaci, M. Shuler and J. Hickman, *J. Lab. Autom.*, 2015, **20**, 107–126.

9 O. Henry, R. Villenave, M. Cronce, W. Leineweber, M. Benz and D. Ingber, *Lab Chip*, 2017, **17**, 2264–2271.

10 M. Odijk, A. van der Meer, D. Levner, H. Kim, M. van der Helm, L. Segerink, J. Frimat, G. Hamilton, D. Ingber and A. van den Berg, *Lab Chip*, 2015, **15**, 745–752.

11 M. W. van der Helm, M. Odijk, J. P. Frimat, A. D. van der Meer, J. C. T. Eijkel, A. van den Berg and L. I. Segerink, *Biosens. Bioelectron.*, 2016, **85**, 924–929.

12 M. W. van der Helm, O. Y. F. Henry, A. Bein, T. Hamkins-Indik, M. J. Cronce, W. D. Leineweber, M. Odijk, A. D. van der Meer, L. I. Segerink and D. E. Ingber, *Lab Chip*, 2019, **19**, 452–463.

13 O. Henry, R. Villenave, M. Cronce, W. Leineweber, M. Benz and D. Ingber, *Lab Chip*, 2017, **17**, 2264–2271.

14 I. Maschmeyer, T. Hasenberg, A. Jaenicke, M. Lindner, A. K. Lorenz, J. Zech, L. A. Garbe, F. Sonntag, P. Hayden, S. Ayehunie, R. Lauster, U. Marx and E. M. Materne, *Eur. J. Pharm. Biopharm.*, 2015, **95**, 77–87.

15 P. Zeller, A. Legendre, S. Jacques, M. J. Fleury, F. Gilard, G. Tcherkez and E. Leclerc, *J. Appl. Toxicol.*, 2017, **37**, 287–295.

16 P. Shah, J. V. Fritz, E. Glaab, M. S. Desai, K. Greenhalgh, A. Frachet, M. Niegowska, M. Estes, C. Jäger, C. Seguin-Devaux, F. Zenhausern and P. Wilmes, *Nat. Commun.*, 2016, **7**, 1–15.

17 Y. I. Wang, H. E. Abaci and M. L. Shuler, *Biotechnol. Bioeng.*, 2017, **114**, 184–194.

18 R. Booth and H. Kim, *Lab Chip*, 2012, **12**, 1784–1792.

19 L. M. Griep, F. Wolbers, B. De Wagenaar, P. M. Ter Braak, B. B. Weksler, I. A. Romero, P. O. Couraud, I. Vermes, A. D. Van Der Meer and A. Van Den Berg, *Biomed. Microdevices*, 2013, **15**, 145–150.

20 O. Y. F. Henry, R. Villenave, M. J. Cronce, W. D. Leineweber, M. A. Benz and D. E. Ingber, *Lab Chip*, 2017, **17**, 2264–2271.

21 P. Shah, J. V. Fritz, E. Glaab, M. S. Desai, K. Greenhalgh, A. Frachet, M. Niegowska, M. Estes, C. Jäger, C. Seguin-Devaux, F. Zenhausern and P. Wilmes, *Nat. Commun.*, 2016, **7**, 1–15.

22 C. Probst, S. Schneider and P. Loskill, *Curr. Opin. Biomed. Eng.*, 2018, **6**, 33–41.

23 T. S. Khire, B. J. Nehilla, J. Getpreecharsawas, M. E. Gracheva, R. E. Waugh and J. L. McGrath, *Biomed. Microdevices*, 2018, **20**(1), 11.

24 C. M. Lo, C. R. Keese and I. Giaever, *Exp. Cell Res.*, 1999, **250**, 576–580.

25 O. Y. F. Henry, R. Villenave, M. J. Cronce, W. D. Leineweber, M. A. Benz and D. E. Ingber, *Lab Chip*, 2017, **17**, 2264–2271.

26 S. J. Trietsch, E. Naumovska, D. Kurek, M. C. Setyawati, M. K. Vormann, K. J. Wilschut, H. L. Lanz, A. Nicolas, C. P. Ng, J. Joore, S. Kustermann, A. Roth, T. Hankemeier, A. Moisan and P. Vulto, *Nat. Commun.*, 2017, **8**, 262.

27 E. Naumovska, G. Aalderink, C. Wong Valencia, K. Kosim, A. Nicolas, S. Brown, P. Vulto, K. S. Erdmann and D. Kurek, *Int. J. Mol. Sci.*, 2020, **21**, 4964.

28 L. Gijzen, D. Marescotti, E. Raineri, A. Nicolas, H. L. Lanz, D. Guerrera, R. van Vught, J. Joore, P. Vulto, M. C. Peitsch, J. Hoeng, G. Lo Sasso and D. Kurek, *SLAS Technol.*, 2020, **25**, 585–597.

29 M. K. Vormann, L. Gijzen, S. Hutter, L. Boot, A. Nicolas, A. van den Heuvel, J. Vriend, C. P. Ng, T. T. G. Nieskens, V. van Duinen, B. de Wagenaar, R. Masereeuw, L. Suter-Dick, S. J. Trietsch, M. Wilmer, J. Joore, P. Vulto and H. L. Lanz, *AAPS J.*, 2018, **20**(5), 90.

30 J. Vriend, T. T. G. Nieskens, M. K. Vormann, B. T. van den Berge, A. van den Heuvel, F. G. M. Russel, L. Suter-Dick, H. L. Lanz, P. Vulto, R. Masereeuw and M. J. Wilmer, *AAPS J.*, 2018, **20**, 1–13.

31 F. Schutgens, M. B. Rookmaaker, T. Margaritis, A. Rios, C. Ammerlaan, J. Jansen, L. Gijzen, M. Vormann, A. Vonk, M. Viveen, F. Y. Yengej, S. Derakhshan, K. M. de Winter-de Groot, B. Artegiani, R. van Boxtel, E. Cuppen, A. P. A. Hendrickx, M. M. van den Heuvel-Eibrink, E. Heitzer, H. Lanz, J. Beekman, J. L. Murk, R. Masereeuw, F. Holstege, J. Drost, M. C. Verhaar and H. Clevers, *Nat. Biotechnol.*, 2019, **37**, 303–313.

32 A. Petrosyan, P. Cravedi, V. Villani, A. Angeletti, J. Manrique, A. Renieri, R. E. De Filippo, L. Perin and S. Da Sacco, *Nat. Commun.*, 2019, **10**, 1–17.

33 V. van Duinen, D. Zhu, C. Ramakers, A. J. van Zonneveld, P. Vulto and T. Hankemeier, *Angiogenesis*, 2019, **22**, 157–165.

34 V. Van Duinen, A. Van Den Heuvel, S. J. Trietsch, H. L. Lanz, J. M. Van Gils, A. J. Van Zonneveld, P. Vulto and T. Hankemeier, *Sci. Rep.*, 2017, **7**, 1–11.

35 N. R. Wevers, D. G. Kasi, T. Gray, K. J. Wilschut, B. Smith, R. Vught, F. Shimizu, Y. Sano, T. Kanda, G. Marsh, S. J. Trietsch, P. Vulto, H. L. Lanz and B. Obermeier, *Fluids Barriers CNS*, 2018, **15**, 23.

36 A. Moisan, F. Michielin, W. Jacob, S. Kronenberg, S. Wilson, B. Avignon, R. Gerard, F. Benmansour, C. McIntyre, G.

Meneses-Lorente, M. Hasmann, A. Schneeweiss, M. Weisser and C. Adessi, *Mol. Cancer Ther.*, 2018, **17**, 1464–1474.

37 Y. Koo, B. T. Hawkins and Y. Yun, *Sci. Rep.*, 2018, **8**, 1.

38 J. Schindelin, I. Arganda-Carreras, E. Frise, V. Kaynig, M. Longair, T. Pietzsch, S. Preibisch, C. Rueden, S. Saalfeld, B. Schmid, J. Y. Tinevez, D. J. White, V. Hartenstein, K. Eliceiri, P. Tomancak and A. Cardona, *Nat. Methods*, 2012, **9**, 676–682.

39 P. Vulto, S. Podszun, P. Meyer, C. Hermann, A. Manz and G. A. Urban, *Lab Chip*, 2011, **11**, 1596–1602.

40 C. Beaurivage, E. Naumovska, Y. X. Chang, E. D. Elstak, A. Nicolas, H. Wouters, G. van Moolenbroek, H. L. Lanz, S. J. Trietsch, J. Joore, P. Vulto, R. A. J. Janssen, K. S. Erdmann, J. Stallen and D. Kurek, *Int. J. Mol. Sci.*, 2019, **20**, 5661.

41 L. Gijzen, D. Marescotti, E. Raineri, A. Nicolas, H. L. Lanz, D. Guerrera, R. van Vught, J. Joore, P. Vulto, M. C. Peitsch, J. Hoeng, G. Lo Sasso and D. Kurek, *SLAS Technol.*, 2020, **25**, 585–597.

42 G. Muzes, B. Molnár, Z. Tulassay and F. Sipos, *World J. Gastroenterol.*, 2012, **18**, 5848–5861.

43 S. H. Murch, C. P. Braegger, J. A. Walker-Smith and T. T. MacDonald, *Gut*, 1993, **34**, 1705–1709.

44 R. Daig, T. Andus, E. Aschenbrenner, W. Falk, J. Schölmerich and V. Gross, *Gut*, 1996, **38**, 216–222.

45 L. Gijzen, D. Marescotti, E. Raineri, A. Nicolas, H. L. Lanz, D. Guerrera, R. van Vught, J. Joore, P. Vulto, M. C. Peitsch, J. Hoeng, G. Lo Sasso and D. Kurek, *SLAS Technol.*, 2020, **25**, 585–597.

46 J. Yeste, X. Illa, C. Gutiérrez, M. Solé, A. Guimerà and R. Villa, *J. Phys. D: Appl. Phys.*, 2016, **49**, 375401.

47 B. M. Denker and E. Sabath, *J. Am. Soc. Nephrol.*, 2011, **22**, 622–625.